Proceedings of the ASME 2018
International Mechanical Engineering Congress and Exposition
IMECE2018
November 9-15, 2018, Pittsburgh, PA, USA

IMECE2018-88752

DESIGN OF A ROBUST YAW RATE CONTROLLER USING SLIDING MODE CONTROL AND EXTENDED STATE OBSERVER FOR NAVIGATION OF AN AUTONOMOUS GROUND VEHICLE

Suraj Shamrao Borate
Defence Institute of Advanced Technology (DIAT)
Pune, Maharashtra, India

Shubhashisa Sahoo
Center for Artificial Intelligence and Robotics
Bengaluru, Karnataka, India

Devika K Baby
Indian Institute of Technology (IIT), Madras
Chennai, Tamil Nadu, India

Shankar C Subramanian
IIT, Madras
Chennai, Tamil Nadu, India

Kiran K Mangrulkar
DIAT
Pune, Maharashtra, India

ABSTRACT

This paper deals with tracking of desired yaw rate generated by the path planner of an Autonomous Ground Vehicle (AGV) in the presence of unmodeled dynamics, changes in operating conditions and parametric uncertainties. A mathematical model considering the dynamics of the test vehicle and the steering actuator was used for controller design. The estimate of the unknown part of dynamics, called the total disturbance, obtained from the Extended State Observer (ESO) was used by Sliding Mode Controller (SMC) to compensate the actual total disturbance. It was observed that the lower bound on the SMC switching gain depends on the ratio of total disturbance estimation error and assumed known part of the system dynamics. This allows the choice of a low value of SMC switching gain, which in turn resulted in reduced chattering amplitude. Further attenuation in chattering was achieved using a saturation function.

After simulating the designed controller in MATLAB-SIMULINK environment, the controller was validated in IPG: CarMaker® simulation platform over a large operating range by changing the mass distribution of the vehicle, speed of the vehicle, cornering stiffness of the tire and terrain friction coefficient. A look-up table was formulated for the maximum achievable yaw rate at different speeds, i.e., from 5 to 20 m/s, given the maximum steering angle input considering rollover and slip threshold while the terrain friction coefficient was also varied from 0.2 to 0.8. It was observed that the designed controller was robust to changes in operating conditions, parametric uncertainties and unmodeled dynamics.

NOMENCLATURE

Symbol	Description
b	Unknown coefficient of the steering angle
b_0	Known part of b
C_f	Cornering stiffness of the front tire (N/rad)
C_r	Cornering stiffness of the rear tire (N/rad)
d	Total disturbance
$\hat{d}$	Estimate of total disturbance.
F_{yf}	Lateral tire force on the front wheel (N)
F_{yr}	Lateral tire force on the rear wheel (N)
f	An unknown function for the yaw rate
I_z	Yaw moment of inertia of the vehicle (kg.m^2)
k	Switching gain
l_f	Distance of front axle from center of gravity (m)
l_r	Distance of rear axle from center of gravity (m)
m	Mass of the vehicle (kg)
r	Yaw rate of the vehicle (rad/s)
r_d	Desired yaw rate (rad/s)
s	Sliding variable
v	Longitudinal speed of the vehicle (m/s)
x_1	First state in extended state space, same as r
x_2	Second state in extended state space, same as d
$\hat{x}_1$	Estimate ofx_1.
$\hat{x}_2$	Estimate of x_2 same as $\hat{d}$
α_f	Slip angle of the front wheel (rad)
α_r	Slip angle of the rear wheel (rad)
β	Side-slip angle of the vehicle (rad)
δ	Steering angle of the front wheel (rad)
δ_{eq}	Equivalent control

ε	External disturbance
Φ	Angle of rotation of the steering motor shaft (rad)
λ	Sliding surface slope.

INTRODUCTION

Autonomous Ground Vehicles (AGVs) are rapidly finding their way from commercial transportation to defense and even space robotics [1, 2]. An AGV should have the ability to sense the environment, take decisions, plan feasible paths and control its actuators accordingly to follow the path as generated by the vehicle path planner. All these need to be done in real-time and in environments that may change dynamically, for example, encountering unexpected obstacles or disturbances. Ozguner et al. [3] described various drive-by-wire actuators, vehicle hardware, high and low level control systems, sensors and related environmental sensing technologies of Team Terramax and its entry to the Defence Advanced Research Project Agency (DARPA) Grand challenge 2004.

A vehicle perception module (VPM) is required to acquire the states of the AGV such as its position, orientation, velocities and location of obstacles in the environment. The sensor fusion algorithm of the VPM combines the data received from the internal and the external sensors to estimate the states of both the AGV and its environment. Shimchik et al. [4] listed a sensor kit such as Global Positing System (GPS), Inertial Measurement Unit (IMU), wheel odometry, two-dimensional and three-dimensional laser scanners for the prototype development of an autonomous golf cart and demonstrated the navigation of the golf cart model in Gazebo simulator using ROS: an open source robot operating system. The path planner algorithm of the AGV determines the desired velocity and the yaw rate in real time considering the initial configuration of the vehicle, the GPS waypoints and the obstacle points received from the sensory inputs. Roamann et al. [5] presented a Timed-Elastic Bands (TEB) path planner that generates a trajectory after approximating the analytical time-optimal trajectory in a few iterations. Houenou et al. [6] proposed a trajectory prediction method based on constant yaw rate and acceleration motion model for short-term prediction and a prediction based on maneuver recognition for longer-term prediction. The vehicle path tracker provides the desired actuator commands to ensure that the desired velocity and the yaw rate provided by the path planner are tracked. Path tracker uses a control strategy to minimize the error. The vehicle actuation module provides the required actuator signals to the accelerator pedal, brake pedal and steering wheel according to the commands received from the vehicle path tracker.

Path tracking methods that simultaneously track the velocity and yaw rate have been proposed in the literature [7, 8]. Longitudinal motion models can be used for design of velocity control [9]. For navigation between consecutive GPS waypoints in an obstacle free path and if there is a small change in the desired heading angle of the vehicle, then velocity of vehicle can be assumed as constant [10]. But while taking a tighter turn at the junctions, changing the lane, overtaking or avoiding an obstacle in the path, the vehicle path planner provides the desired yaw rate at a constant velocity. As the yaw rate of the vehicle can be measured directly by using an IMU whereas the heading angle of the vehicle is determined by integrating the yaw rate which results reduced accuracy and increased computation and smoother response [11]. In order to avoid the error in determination of heading angle by integrating the yaw rate, it is always better to track the yaw rate of the vehicle for curvilinear motions.

A robust control technique is required as the accuracy of tracking desired yaw rate of the vehicle reduces due to unmodeled dynamics, changes in operating conditions and parametric uncertainties [12]. SMC, by virtue of its sliding mode motion, is an inherently robust control strategy [13]. Talole et al. [14] designed a combination of ESO and feedback linearization based controller and implemented it on a flexible joint manipulator where ESO was used to estimate parametric uncertainties, unmodeled dynamics and external disturbance as a single term called the total disturbance which was compensated using control.

A robust yaw rate controller is proposed using combination of two robust control techniques Extended State Observer (ESO) and Sliding mode control (SMC). The controller was designed and simulated in MATLAB SIMULINK environment. Then, the designed controller was evaluated in IPG: CarMaker® simulation platform on a tested realistic model for various operating conditions to demonstrate its robustness. The rest of this paper is organized as follows: the next section describes the dynamic mathematical model of the AGV. In the subsequent section, equations for SMC and ESO are derived. The sections on SMC and ESO are followed by sections describing the modeling of steering actuator and description of vehicle parameters and tire parameters. Finally, the open-loop and closed-loop results are presented.

THE VEHICLE MODEL

The test vehicle under study has an Ackerman-like steering mechanism and only the front wheel of the vehicle is steerable. Figure 1 shows schematic representation of bicycle model.

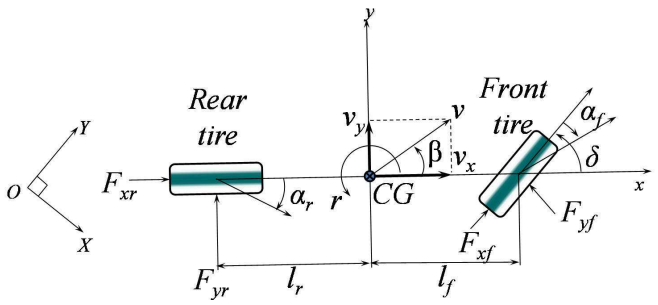

Fig. 1: Dynamic bicycle model.

Considering the mass distribution at the left and the right side of the vehicle to be nearly same, a dynamic bicycle model was used for simplicity. The forces acting at the left and right tires combined together and transferred to an imaginary tire placed at the middle of the axle. In addition to this, the longitudinal speed of the vehicle was assumed to be constant for the bicycle model. The lateral displacement is along body frame *y*-axis and yaw angle is the angle between the longitudinal axis of the vehicle, i.e., *x*-axis and the global *X*-axis. Considering the steering angle, δ to be small, the governing equations for the bicycle model can be represented as,

$$m\left(\dot{v}_y(t)+v_x(t)r(t)\right)=F_{yf}(t)+F_{yr}(t) \tag{1}$$

and

$$I_z\dot{r}(t)=l_f F_{yf}(t)-l_r F_{yr}(t). \tag{2}$$

It has been verified experimentally that when the slip-angles of the tire is less than 5°, the lateral force is proportional to the slip angle of the tire [15]. The lateral forces acting on the front and rear wheels are represented as

$$F_{yf}(t)=C_f\alpha_f(t) \text{ and } F_{yr}(t)=C_r\alpha_r(t). \tag{3}$$

The slip angles at the front and rear tires can be derived as,

$$\alpha_f(t)=\delta(t)-\left(\frac{v_y(t)+l_f r(t)}{v_x}\right) \text{ and } \alpha_r(t)=-\left(\frac{v_y(t-l_r r(t)}{v_x}\right). \tag{4}$$

Using equations from (1) to (4), the governing equations become

$$m\dot{v}_y(t)+\left(\frac{C_f+C_r}{v_x}\right)v_y(t)+\left(mv_x+\frac{C_f l_f-C_r l_r}{v_x}\right)r(t)=C_f\delta(t) \tag{5}$$

and

$$I_z\dot{r}(t)+\left(\frac{C_f l_f-C_r l_r}{v_x}\right)v_y(t)+\left(\frac{C_f {l_f}^2+C_r {l_r}^2}{v_x}\right)r(t)=C_f l_f\delta(t). \tag{6}$$

For the purpose of simulation, the actual yaw rate, *r* is obtained from the equation (6) and the desired yaw rate, r_d is assumed to be decided by the vehicle path planner. Overview of the control structure is explained in the next section.

SYSTEM CONTROL STRUCTURE

The block diagram of the system control structure comprising of mathematical model of the vehicle, ESO, SMC and steering angle controller is shown in Fig. 2.The total disturbance, $\hat{d}$ is estimated by the ESO considering steering wheel angle, δ and the actual yaw rate, *r* of the vehicle. The SMC generates the desired steering angle input to the vehicle using the estimates of the total disturbance and the tracking error in yaw rate and the derivative of desired yaw rate at any particular velocity. In order to track the desired steering angle generated by the steering a proportional steering angle controller is used. The design of the controller is discussed in the next section.

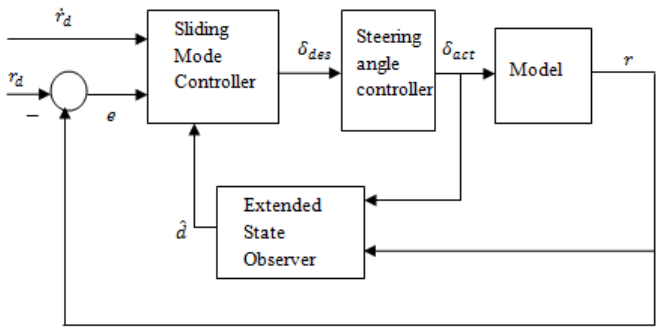

Fig. 2: System control structure.

SLIDING MODE CONTROLLER

The yaw dynamics of the system derived in equation (6) may be rewritten as

$$\dot{r}(t)=f(t)+\varepsilon(t)+b\delta(t), \tag{7}$$

where, *f* is an unknown dynamic function which may be linear or nonlinear and time-varying, ε is the external disturbances and *b* is the coefficient of the steering angle. Known part of *b* is assumed to be $b_0 = 2l_fC_f/I_z$. Now, equation (7) can be modified as

$$\dot{r}(t)=f(t)+\varepsilon(t)+(b-b_0)\delta(t)+b_0\delta(t). \tag{8}$$

On combining the unknown terms of system nonlinearities, parametric uncertainties and disturbances as the total disturbance *d*, equation (8) can be written as

$$\dot{r}(t)=d(t)+b_0\delta(t), \tag{9}$$

where, $d=f+\varepsilon+(b-b_0)\delta$. Considering the error in the yaw rate *e*, as the difference between the desired yaw rate, r_d and the actual yaw rate *r*, the switching function, *s(t)* for the sliding mode controller design can be defined as

$$s(t)=\lambda\left(r_d(t)-r(t)\right), \tag{10}$$

where, λ is a positive constant. To track the desired yaw rate, the system trajectory should reach and remain on the sliding surface, *s(t)=0*. The motion of the system trajectory on the

sliding surface is known as sliding mode motion. In order to maintain sliding mode motion the derivative of switching function,

$$\dot{s}(t) = \lambda\left(\dot{r}_d(t) - \dot{r}(t)\right) \tag{11}$$

should be equal to zero. This is achieved using equivalent control, δ_{eq} [16]. On substituting $\dot{r}$ from equation (9) in equation (11),

$$\dot{r}_d(t) - \left(d(t) + b_0\delta(t)\right) = 0\,. \tag{12}$$

However, the total disturbance, d is unknown. So, the estimate of the total disturbance, $\hat{d}$ is used to derive the equivalent control, δ_{eq},

$$\delta_{eq}(t) = -\left(\frac{\dot{r}_d(t) - \hat{d}(t)}{b_0}\right). \tag{13}$$

In order to make the system trajectory to reach the sliding surface, a bang-bang control structure, *k sgn(s)* is used [16] along with the equivalent control. Hence, the total control equation is of the form

$$\delta(t) = \delta_{eq}(t) + k\,\mathrm{sgn}(s), \tag{14}$$

where, k is the switching gain and,

$$\mathrm{sgn}(s)\begin{cases} = 1, \text{ when } s > 0, \\ = 0, \text{ when } s = 0, \\ = -1, \text{ when } s < 0. \end{cases} \tag{15}$$

Hence, the SMC equation becomes

$$\delta(t) = \left(\frac{\dot{r}_d(t) - \hat{d}(t)}{b_0}\right) + k\,\mathrm{sgn}(s)\,. \tag{16}$$

The term *k sgn(s)* in the control equation introduces high frequency control switching in the vicinity of the sliding surface. This undesirable phenomenon is known as chattering [16]. This is an undesirable phenomenon as far as practical systems are concerned as the high frequency control switching often results in actuator damage. The switching gain, k is proportional to the chattering amplitude. Hence, it is desired that k should be as small as possible. The condition for choosing k is obtained by applying Lyapunov stability criterion, i.e.,

$$\frac{d}{dt}\frac{1}{2}s(t)^2 < 0\,. \tag{17}$$

Therefore,

$$s(t)\dot{s}(t) < 0\,, \tag{18}$$

Substituting $\dot{s}$ from equation (11) in equation (18),

$$s(t)\lambda\left[\dot{r}_d(t) - \dot{r}(t)\right] < 0\,. \tag{19}$$

Now, substituting $\dot{r}$ from equation (9) in equation (19),

$$s(t)\left[\dot{r}_d(t) - d(t) - b_0\delta(t)\right] < 0\,. \tag{20}$$

Depending on vehicle's response time, the desired yaw rate is kept at constant value for sufficient amount of time. Hence, maneuvers are designed as series of step functions. Hence it is assumed that $\dot{r}_d = 0$. Now on substituting equation (16) in equation (20)

$$s(t)\left[\hat{d}(t) - d(t) - kb_0\,\mathrm{sgn}(s)\right] < 0\,. \tag{21}$$

Substituting *k sgn(s)* as $|s|$ in equation (21)

$$s(t)\left[\hat{d}(t) - d(t)\right] < kb_0|s|\,. \tag{22}$$

Therefore,

$$\left|\frac{\hat{d}(t) - d(t)}{b_0}\right| < k\,, \tag{23}$$

where, $\hat{d} - d$ is the total disturbance estimation error. Thus, the value of switching gain, k should be greater than the ratio of magnitude of estimation error and the known part of coefficient of the steering angle, b_0. Since b_0 is inversely proportional to k, assuming high value of b_0 leads to chattering attenuation. The equivalent control in equation(13) also includes estimate of total disturbance, which compensates for the actual total disturbance. Thus, both the switching portion of the control equation and equivalent control contribute to dealing with uncertainties unlike conventional SMC where only switching portion contributed to robustness. Since equivalent control contributes major share in uncertainty compensation the gain in the switching portion of total control equation can be smaller which leads to chattering attenuation.

Saturation Function

The term *k sgn(s)* in equation (16) is responsible for forcing the system to the sliding surface, $s(t) = 0$. But, due to inherent delay in the discrete implementation, it introduces chattering phenomenon. This effect is undesirable as it may cause damage to actuators. Chattering attenuation was obtained by choice of low value of k in control equation to some extent. Further attenuation can be obtained by using saturation function

instead of sign function in equation (16). Hence the control equation becomes

$$\delta(t) = \left(\frac{\dot{r}_d(t) - \hat{d}(t)}{b_0} \right) + k sat(s) . \quad (24)$$

where, $\text{sat}(s) = s \quad if\ |s| \leq 1,$
$\text{sat}(s) = \text{sgn}(s) \quad if\ |s| > 1.$

Use of saturation function in conventional sliding mode control technique adversely affects the robustness and accuracy of the controller. But in the approach presented, robustness achieved due to real-time estimation of uncertainties by the extended State Observer compensates for the loss of robustness caused by the use of saturation function. Thus chattering attenuation was achieved without compromising the robustness property.

EXTENDED STATE OBSERVER (ESO)

In order to design ESO for the estimation of the total disturbance, consider the dynamics of the system as

$$\dot{x}_1(t) = \dot{r}(t) = d(t) + b_0 \delta(t) \quad (25)$$

The output of the system is yaw rate

$$y(t) = x_1(t) = r(t) \quad (26)$$

While the yaw rate, r can be measured, the total disturbance, d has to be estimated. The extended state observer technique involves considering $d$as an additional or extended state [18]. Thus $d = x_2$ and $\hat{d} = \hat{x}_2$. Thus

$$\dot{\hat{x}}_1(t) = \hat{x}_2 + b_0 \delta(t) + l_1 \left(y(t) - \hat{x}_1(t) \right) \quad (27)$$

$$\dot{\hat{x}}_2(t) = l_2 \left(y(t) - \hat{x}_1(t) \right) \quad (28)$$

Equations (27) and (28) can be represented in state space form as

$$\dot{\hat{\boldsymbol{x}}} = \boldsymbol{A}\hat{\boldsymbol{x}}(t) + \boldsymbol{b}\delta(t) + \boldsymbol{l}[y(t) - \hat{\boldsymbol{x}}(t)]$$

$$y = \boldsymbol{c}\hat{\boldsymbol{x}}(\boldsymbol{t}) \quad (29)$$

where, $\hat{\boldsymbol{x}} = \begin{bmatrix} \hat{x}_1 \\ \hat{x}_2 \end{bmatrix}$, $\dot{\hat{\boldsymbol{x}}} = \begin{bmatrix} \dot{\hat{x}}_1 \\ \dot{\hat{x}}_2 \end{bmatrix}$, $\boldsymbol{A} = \begin{bmatrix} 0 & 1 \\ 0 & 0 \end{bmatrix}$, $\boldsymbol{b} = \begin{bmatrix} b_0 \\ 0 \end{bmatrix}$, $\boldsymbol{l} = \begin{bmatrix} l_1 \\ l_2 \end{bmatrix}$ and $\boldsymbol{c} = [1 \quad 0]$.

where l_1 and l_2 are observer gains that can be obtained by pole placement. For desired vehicle performance observer poles were placed at -20 and -15. Hence, abiding by equation (24), k was chosen to be 0.001.

MODELING OF THE STEERING ACTUATOR

The presence of any actuator causes delay and alters output characteristics and also introduces limits on maximum and minimum possible input to the system. Sahoo et al. [18] observed that the steering actuator dynamics needs to be considered when the time taken to steer the front wheel is same as the order of the heading angle response of the vehicle. It was found that the front wheel of the vehicle steers at a rate of approximately 10 °/s. A proportional controller was designed using the model of steering actuator derived analytically from basic governing equations. This controller minimizes the difference between the actual steering angle of the vehicle and the steering angle generated by SMC.

TEST VEHICLE

In earlier work, Sahoo et al. [19] used a front wheel steered battery-operated vehicle as the test vehicle after converting it to drive-by-wire. Figure 3 shows the test vehicle and the sensors mounted on it. To gain confidence before real-time implementation on the actual test vehicle and constrained by safety reasons, the performance of the controller was tested in IPG: CarMaker® simulation platform. The specifications of the test vehicle listed in Table 1 were used for simulation.

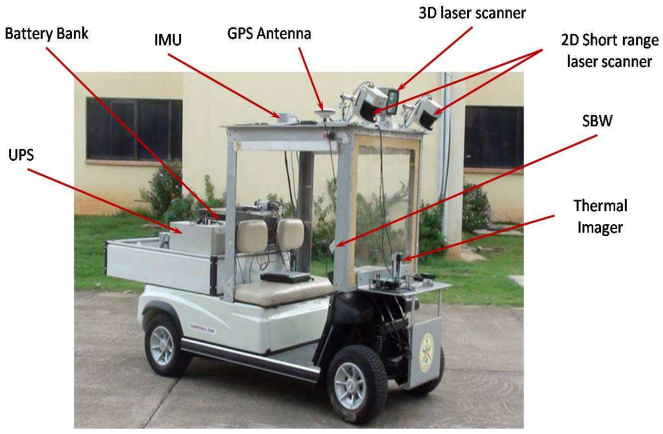

Fig. 3: Test Vehicle.

Table 1. Parameters of the test vehicle.

Parameter	Value	Unit
Mass at front-left wheel (m_{fl})	158	kg
Mass at front-right wheel (m_{fr})	137	kg
Mass at rear-left wheel (m_{rl})	360	kg
Mass at rear-right wheel (m_{rr})	269	kg
Mass of the vehicle (m)	924	kg
Wheelbase (l)	1.93	m
Location of CG from front axle (l_f)	1.31	m
Location of CG from rear axle (l_r)	0.62	m
Moment of inertia (I_z)	932	kgm^2

Position, orientation, linear and angular velocities of the vehicle are measured by using a tightly coupled GPS and IMU. The angular position of the steering actuator is measured using the encoder attached to it. The angular displacement of the steering actuator is converted to the front wheel steering angle using the gear ratio of the rack and pinion mechanism. The mass and moment of inertia of the vehicle are calculated after measuring the vertical load on each wheel.

Estimation of cornering stiffness of tires

Accurate estimation of cornering stiffness requires large number of experiments and expensive equipment. Hence, a mathematical model was derived by Hewson [20] using the information available in the tire specifications. Cornering stiffness of the tire used in the test vehicle was calculated as 132600 N/rad using the Hewson's formula. Though the cornering stiffness may vary with vertical load, it was assumed to be equal for all tires with same specifications.

RESULTS

A robust controller was designed in the previous section to track the desired yaw rate. The parameters of the test vehicle mentioned in Table 1 were used to develop the mathematical model of the vehicle in MATLAB SIMULINK environment. Then, the same parameters were used to evaluate the controller in IPG: CarMaker® for a J-turn or constant yaw rate maneuver. The maximum possible steering angles and desired yaw rates that can be achieved by the controller such that the vehicle does not slip or rollover were tabulated for different speeds and terrain friction coefficient, and are listed in Table 2.

Table 2. Maximum possible steering angles at various speed of the vehicle considering the rollover and slip threshold on different terrains.

Vehicle speed (m/s)	Terrain friction coefficient	Maximum steering angle (°)	Maximum yaw rate (°/s)
5	0.8	16.1	46.2
	0.6	18.0	48.0
	0.4	16.3	40.1
	0.2	15.5	21.5
10	0.8	5.5	24.3
	0.6	5.0	24.5
	0.4	5.5	22.2
	0.2	5.1	11.5
15	0.8	2.3	13.2
	0.6	2.1	13.2
	0.4	2.5	14.6
	0.2	1.2	7.6
20	0.8	0.8	9.7
	0.6	1.3	10.5
	0.4	1.3	10.1
	0.2	0.7	5.7

Adhering by the saturation limits on steering angle mentioned in Table 2various open-loop tests such as variation in the speed of the vehicle, cornering stiffness, mass distribution of the vehicle, terrain friction coefficient were tested in open loop. In order to study robustness of the designed controller, closed loop tests were also carried out under same operating conditions as open loop tests.

Effect of variation in speed on yaw rate

Figure 4 shows the simulated characteristics of yaw rate in open-loop at a steering angle of 0.5° for speed ranging from 0 to 20 m/s. It is observed that the yaw rate varies from 1.9 °/s to 7.1 °/s as the longitudinal speed of the vehicle varies from 5 m/s to 20 m/s. In spite of these variations in the open loop, the closed loop controller was able to track yaw rate of 10°/s for the entire operating range of 0 to 20 m/s as shown in Fig. 5.

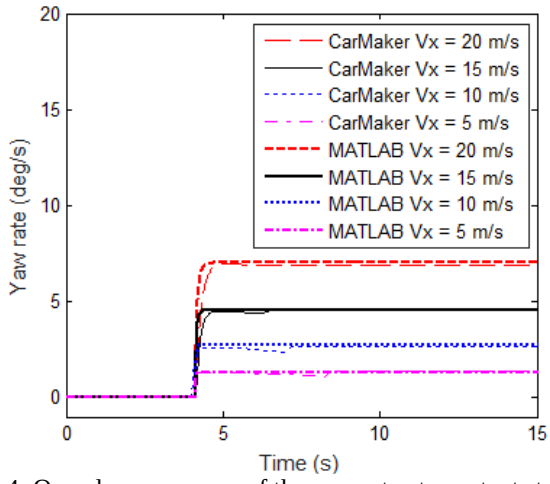

Fig. 4: Open loop response of the yaw rate at constant steering angle of 0.5° for various speeds of the vehicle.

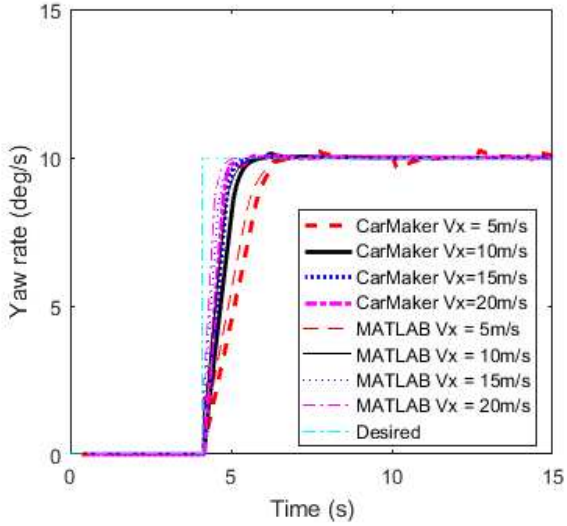

Fig. 5: Closed loop response to track the desired yaw rate of 10°/s at various speeds.

To validate the performance of the designed controller, tests were conducted in IPG: CarMaker® and the results were compared in Fig. 5 and Fig. 6. While tracking a desired yaw rate of 10°/s at 10 m/s, an overshoot of 1 percent was noticed and the rise time was less than 2 s. Corresponding response of the steering angles using the controller are plotted in Fig. 6. It was observed that requirement of steering angle reduced at higher speeds and steering angle is within the safe limits.

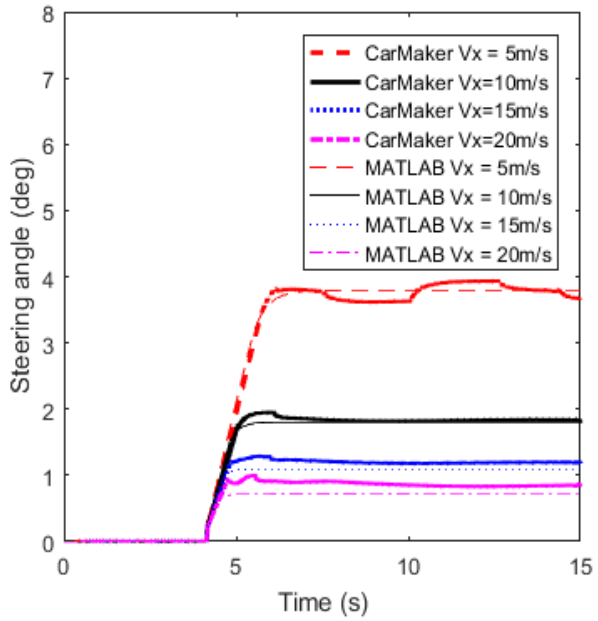

Fig. 6: Closed loop steering angle response at various speeds.

Effect of variation of Cornering Stiffness on yaw rate

Hewson's formula was used to calculate the value of cornering stiffness. However, he concluded in his study that this tire model has a confidence level of 95 percent that the estimated cornering stiffness is within ±30 percent of the actual measured value [20]. Also, the cornering stiffness may change in real operating situations due to the vertical load on the vehicle, terrain friction coefficient and also due to the unevenness of the terrain surface. So, the yaw rate achieved at different cornering stiffness values such as 66300 N/rad (0.5 times of estimated C_f), 132600 N/rad (same as estimated C_f) and 198900 N/rad (1.5 times of estimated C_f) at the speed of 10 m/s for a steering angle of 5° is shown in Fig. 7. The closed loop response of the yaw rate plotted in Fig. 8 shows that the design controller was able to track desired yaw rate of 10°/s despite the cornering stiffness changes by ±50 percent of the estimated value. Corresponding closed loop steering angles are plotted in Fig. 9.

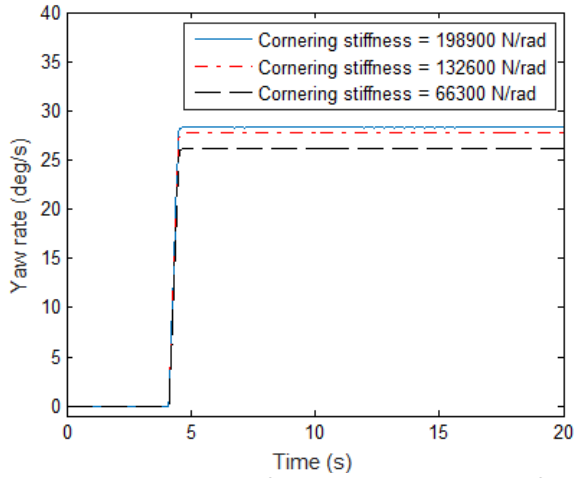

Fig. 7: Open loop response of the yaw rate at a speed of 10 m/s for various cornering stiffnesses.

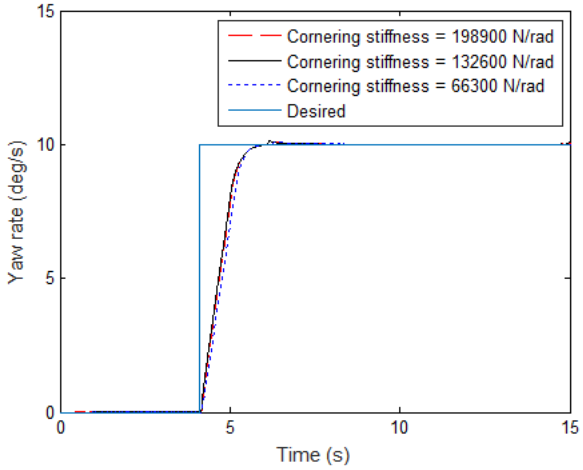

Fig. 8: Closed loop response to track the desired yaw rate of 10°/s at different cornering stiffness.

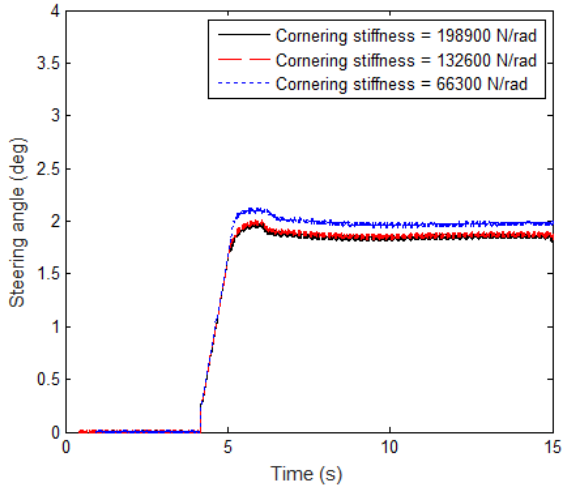

Fig. 9: Closed loop steering angle response at different cornering stiffness of the tire.

Effect of variation of mass-distribution on yaw rate

To check the performance of the designed controller for change in mass distribution, an additional mass of 100 kg was added at front and rear side of vehicle at an operating speed of 10 m/s. For a steering angle input of 5°, the response of the yaw rate is plotted in Fig.10.When the mass at front axle of the vehicle was increased by 100 kg, the yaw rate, *r* reduced from 27.7 to 27.4 °/s and when a mass of 100 kg was added at the rear axle, it was observed that the yaw rate increased to 28.2 °/s. The closed loop yaw rate response is plotted in Fig. 11 and it is observed that the controller was able to track a desired yaw rate of 10°/s efficiently for different mass distribution of the vehicle.

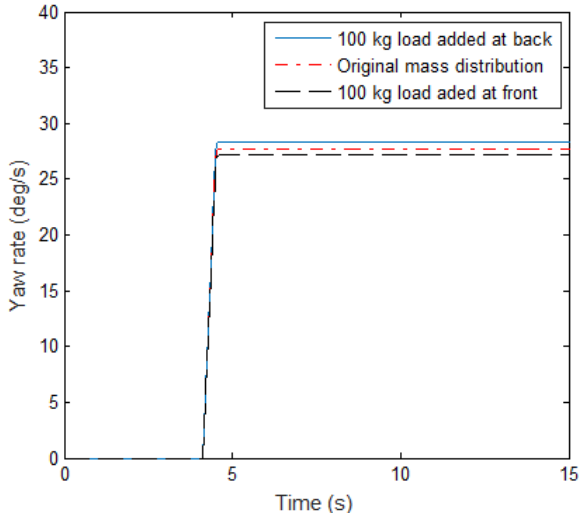

Fig. 10: Open loop response of the yaw rate at a speed of 10 m/s for varying mass distribution of the vehicle.

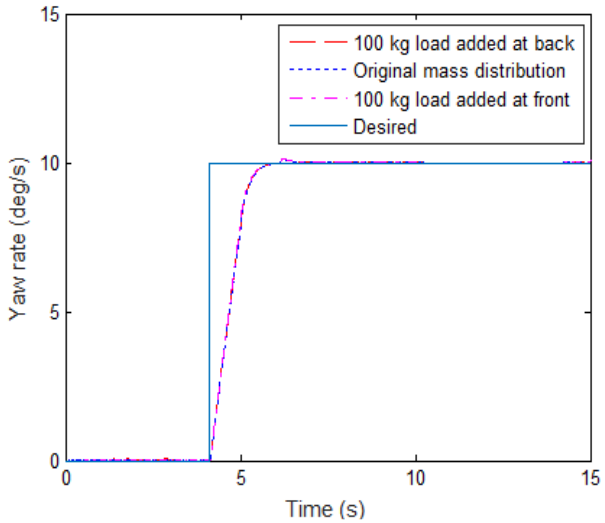

Fig. 11: Closed loop response to track the desired yaw rate of 10 °/s at different mass distribution of the vehicle.

Effect of terrain friction coefficient on yaw rate

For the evaluation of the controller under the influence of terrain friction coefficient, the closed loop yaw rate response was plotted for different terrain friction coefficients such as 0.2, 0.4, 0.6 and 0.8. These tests were carried out at a speed of 10 m/s and the designed controller was evaluated to track a desired yaw rate of 10°/s. The closed loop yaw rate response is shown in Fig. 12 and it was found that the controller was robust enough to track the desired yaw rate at all conditions descried here. However, for a low terrain friction coefficient, slipping of the vehicle occurs. But, it was observed from Fig. 13 that the slip angles of the vehicle were well within ±5 ° for all cases mentioned above.

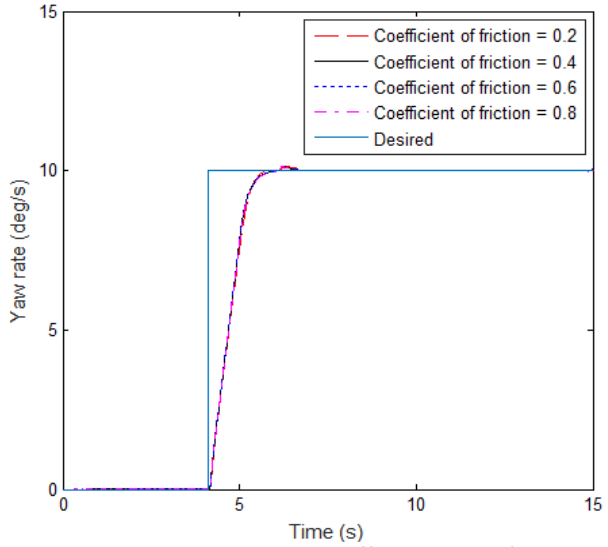

Fig. 12: Tracking yaw rate at different terrain friction coefficient.

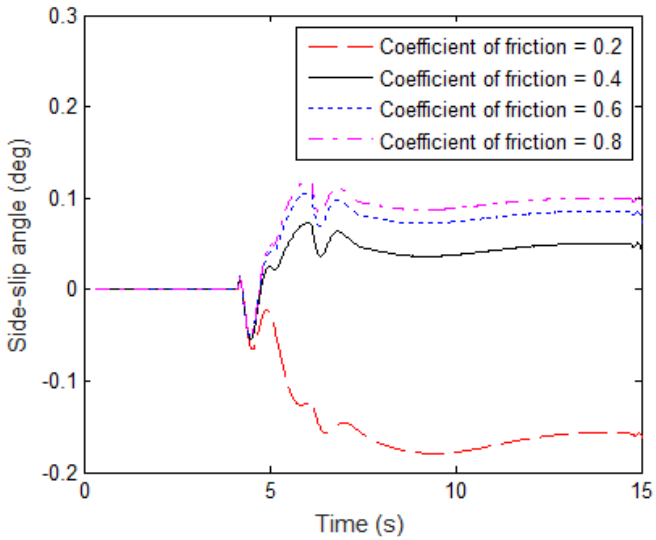

Fig. 13: Side-slip angle at different terrain friction coefficients while tracking yaw rate of 10°/s at velocity 10 m/s

CONCLUSION

A robust yaw rate controller using the combination of sliding mode control and extended state observer was presented in this paper. Unlike the conventional SMC where only the switching portion of the control equation contributes for robustness, the equivalent control also provides robustness as it compensates the uncertainties using the estimate of total disturbance provided by ESO. This reduces the requirement on the switching gain, *k*; as a result chattering attenuation was achieved.

The controller was evaluated using a J-Turn Maneuver in IPG:CarMaker® for accurate and robust tracking of yaw rate at different terrain friction coefficients varying from 0.2 to 0.8, different speeds from 5 m/s to 20 m/s, by varying cornering stiffness value by ± 50 percent and by changing mass distribution by adding 100 kg load at front or rear alternately. While tracking a desired yaw rate of 10°/s at 10 m/s, an overshoot of 1 percent was noticed and the rise time was less than 2 s.

Following are some features of the proposed control strategy:

- The lower bound on switching gain of the presented control equation is small, which results in smaller chattering amplitude. While tracking 10°/s yaw rate at a speed of 10 m/s, chattering amplitude was only 0.05°.
- Further attenuation in chattering phenomenon was achieved using saturation function instead of sign function.
- The controller designed was found to be robust to parametric changes and different operating conditions.

For future work, the developed controller will be implemented on an AGV in real time.

ACKNOWLEDGMENT

The authors thank the Director, CAIR for granting permission to publish the results of this research. The authors also thank the Incubation Center for Automation, Instrumentation and Automobile at the Department of Engineering Design, IIT Madras, established with assistance of the Ministry of Skill, Development and Entrepreneurship, Government of India, for providing access to the IPG:CarMaker® vehicle simulation software.

REFERENCES

[1] Ibanez-Guzman, J., Jian, X., Malcolm, A., Gong, Z., Chan, C. W. and Tay, A., 2004, "Autonomous armoured logistics carrier for natural environments", Proceedings of the IEEE/RSJ International conference on Intelligent Robots and Systems (IROS), Sendai, Japan.

[2] Iagnemma, K., Kang, S., Brooks, C. and Dubowsky S., 2003, "Multi-Sensor Terrain Estimation for Planetary Rovers", Proceeding of the 7thInternational Symposium on Artificial Intelligence, Robotics and Automation in Space, Nara, Japan.

[3] Ozguner, U., Redmill, K. A. and Broggi A., 2004, "Team TerraMax and the DARPA grand challenge: A general overview", Proceeding of the IEEE Intelligent Vehicles Symposium, Parma, Italy.

[4] Shimchik, I., Sagitov, A., Afanasyev, I., Matsuno F. and Magid, E., 2016, "Golf cart prototype development and navigation simulation using ROS and Gazebo", Proceedings of the International conference on Measurement Instrumentation and Electronics, MATEC Web Conferences 75, 09005.

[5] Rosmann, C., Hoffmann, F. and Bertram, T., 2015, "Timed-elastic-bands for time-optimal point-to-point nonlinear model predictive control", Proceedings of the European Control Conference (ECC), Linz, Austria.

[6] Houenou, A., Bonnifait,P., Cherfaoui,V. and Yao W., 2013, "Vehicle Trajectory Prediction based on Motion Model and Maneuver Recognition" Proceedings of the IEEE/RSJ International conference on Intelligent Robots and Systems (IROS), Tokyo, Japan.

[7] Attia, R., Orjuela, R. & Basset, M., 2014, "Combined longitudinal and lateral control for automated vehicle guidance", Vehicle System Dynamics: International Journal of Vehicle Mechanics and Mobility, Vol. 52, No. 2, pp. 261-279.

[8] Yuanqing, X., Pu, F., Li, S. and Gao, Y., G., 2016, "Lateral path tracking control of autonomous land vehicle based on ADRC and differential flatness", IEEE Transactions on Industrial Electronics, Vol. 63, No. 5, pp. 3091-3099.

[9] Schubert, R., Richter E. and Wanielik, G., 2008, "Comparison and evaluation of advanced motion models for vehicle tracking", Proceedings of the 11thInternational conference on Information Fusion, Colonge, Germany.

[10] Sahoo, S., Subramanian, S. C. and Srivastava, S., 2016, "Evaluation of transient response and implementation of a heading angle controller for an autonomous ground vehicle", Proceedings of the Institution of Mechanical Engineers, Part D: Journal of Automobile Engineering, Vol. 230, No. 8, pp. 1040-1056.

[11] Janbakhsh, A. A., Khaknejad, M. B. and Kazemi, R., 2013, "Simultaneous vehicle-handling and path-tracking improvement using adaptive dynamic surface control via a steer-by-wire system", Proceedings of the Institution of Mechanical Engineers, Part D: Journal of Automobile Engineering, Vol. 227, No. 3, pp. 345-360.

[12] Oreh, S. H. T., Kazemi, R. and Azadi, S., 2014, "A sliding-mode controller for directional control of articulated heavy vehicles", Proceedings of the Institution of Mechanical Engineers, Part D: Journal of Automobile Engineering, Vol. 228, No. 3, pp. 245-262.

[13] Utkin, V. I., 1977, "Variable structure systems with sliding modes", IEEE Transactions on Automatic Control, Vol, 22, No, 2, pp. 212-222.

[14] Talole, S. E., Kolhe, J. P. and Phadke, S. B., 2009, "Extended-state-observer-based control of flexible-joint

system with experimental validation", IEEE Transactions on Industrial Electronics, Vol. 57, No. 4, pp. 1411-1419.
[15] Bakker, E., Nyborg, L. and Pacejka, H. B., 1987, "Tire modeling for use in vehicle dynamics studies", SAE paper 870421.
[16] Slotine, J. E. and Li, W., 1991, Applied nonlinear control, Prentice Hall International Editions, pp. 276-310.
[17] Kori, D. K., Kolhe, J. P. and Talole, S. E., 2014, "Extended state observer based robust control of wing rock motion", Aerospace Science and Technology, Vol. 33, pp. 107–117.
[18] Sahoo, S., Subramanian, S. C., Mahale, N. and Srivastava, S., 2015, "Design and development of a heading angle controller for an unmanned ground vehicle", International Journal of Automotive Technology, Vol. 16, No. 1, pp. 27-37.
[19] Sahoo, S., Subramanian, S. C. and Srivastava, S., 2014, "Sensitivity analysis of vehicle parameters for heading angle control of an unmanned ground vehicle", Paper No.IMECE2014-39685, Proceedings of the ASME International Mechanical Engineering Congress Exposition, Montreal, Canada.
[20] Hewson, P., 2005, "Method of estimating tire cornering stiffness from basic tire information," Proceedings of the Institution of Mechanical Engineers, Part D: Journal of Automobile Engineering, Vol. 219, pp. 1407-1412.